



# Highly fluorescent 3-perylenyldiphenylphosphane compounds: An experimental and theoretical study

J. Emilio Expósito<sup>a</sup>, Sergio Lentijo<sup>a</sup>, Gabriel Aullón<sup>b</sup>, Manuel Bardají<sup>a,\*</sup>,  
Jesús A. Miguel<sup>a,\*\*</sup>

<sup>a</sup> IU CINQUIMA/Química Inorgánica, Facultad de Ciencias, Universidad de Valladolid, 47071, Valladolid, Spain

<sup>b</sup> Departament de Química Inorgànica i Orgànica (Secció de Química Inorgànica) and Institut de Química Teòrica i Computacional, Universitat de Barcelona, 08028, Barcelona, Spain

## ARTICLE INFO

**Keywords:**  
Phosphane  
Perylene  
Dye  
Fluorescent  
Gold  
Palladium

## ABSTRACT

The perylene derivative, 3-perylenyldiphenylphosphane (PPh<sub>2</sub>Per, **1**), was prepared and used to synthesize the oxidized P(V) compounds A = PPh<sub>2</sub>Per (A = O (**2**); A = S (**3**)). Substitution reactions led to mononuclear gold(I) complexes [AuX(PPh<sub>2</sub>Per)] (X = Cl (**4**); X = C<sub>6</sub>F<sub>5</sub> (**5**)), [AuX(S=PPh<sub>2</sub>Per)] (X = Cl (**6**); X = C<sub>6</sub>F<sub>5</sub> (**7**)) and palladium(II) complexes *trans*-[Pd(C<sub>6</sub>F<sub>5</sub>)<sub>2</sub>(PPh<sub>2</sub>Per)<sub>2</sub>] (**8**). X-ray single crystal studies of compounds **5** and **7** confirmed the expected structures. The UV–Vis absorption spectra display intense peaks in the visible region with maxima from 454 to 461 nm. A DFT study was performed for the absorption spectra of ligands and complexes, showing that the lowest most intense transition is a HOMO → LUMO transition in the perylene core, although affected by functional group and metallic fragment. The ligands and their complexes are fluorescent in solution, due to the perylene fragment, showing an emission in the range 450–550 nm, with maxima from 467 to 472 nm. Quantum yield starts at 13 % for the phosphane and increases dramatically to the range of 63–87 % after oxidation or coordination to a metal fragment. This work illustrates how the PET effect can be used to recover the initial extremely intense emission of free unfunctionalized perylene ring system.

## 1. Introduction

Perylene compounds are fluorescent dyes with excellent chemical and photochemical stability. They show strong absorption of visible light and high fluorescence quantum yields due to electronic transitions centered at the perylene core. As a consequence of these exceptional properties, they have been employed as industrial pigments [1], as liquid crystals [2,3], in electronic and optical applications [4–9], for highly fluorescent J-aggregates [10,11], in thin films [12,13] and in polymers [14,15].

Phosphane ligands have been widely studied due to their versatility to control their electronic and steric environment, which is very useful to create structural diversity and an efficient change in the photo-physical properties [16–18].

Under these premises, various arylphosphanes derived from aromatic polycycles such as anthracene, phenanthrene or hetero-arylphosphanes have been described, and then, oxidized or coordinated to change their optical properties [19–23]. The incorporation of heavy

atom such as gold(I), to the 9-diphenylphosphinophenanthrene changes the phenanthrene fluorescent behavior to phosphorescent [24]. The phosphorescence of the pyrenyl ring is strongly enhanced by the heavy atom effect of the Pt ion in pyrenyl phosphanes, although this effect depends on the phosphane and metal position in the pyrene core [25]. These phosphane ligands can coordinate a metal, access to the electronic density of the  $\pi$  system by the metal impacts dramatically the photo-physical properties [26–28].

The photoinduced electron transfer (PET) mechanism is well documented for organic probes, where a lone pair of electrons in the receptor quenches the fluorophore emission. Binding of metal ions through the lone pair of electrons in the receptor implies a lower energy for the orbital, which inhibits electron transfer to the fluorophore HOMO, and therefore leads to fluorescence enhancement: an off-on fluorescent chemosensor [29–32].

Phosphane ligands containing a  $\pi$ -system have been used as fluorosensors in biological systems [33,34]. Actually, 3-perylenyldiphenylphosphane was prepared in order to be used as biological luminescent

\* Corresponding author.

\*\* Corresponding author.

E-mail address: [mbardaji@uva.es](mailto:mbardaji@uva.es) (M. Bardají).

<https://doi.org/10.1016/j.dyepig.2025.112690>

Received 10 December 2024; Received in revised form 2 February 2025; Accepted 2 February 2025

Available online 4 February 2025

0143-7208/© 2025 The Authors. Published by Elsevier Ltd. This is an open access article under the CC BY-NC-ND license (<http://creativecommons.org/licenses/by-nc-nd/4.0/>).

probe for lipid peroxidation instead of pyrenylphosphane [35,36]. Now, excitation occurs with visible light instead of the most energetic UV light, which is more convenient for biological samples.

We report the chromophore ligand 3-perylenyldiphenylphosphane, its oxidized species and the coordination compounds with gold(I) and palladium(II). This set of compounds, allow us to study in depth their optical properties, particularly their intense color and emission properties. Theoretical calculations were carried out to support the transition assignments.

## 2. Results and discussion

### 2.1. Syntheses and structures

The syntheses of the ligand 3-perylenyldiphenylphosphane (PPh<sub>2</sub>Per) (1), its oxide (2), its sulfide (3) and their metal complexes are outlined in Scheme 1. The phosphane PPh<sub>2</sub>Per (1) was obtained by a modified method: addition of BuLi to a solution of 3-bromoperylene precursor in THF at  $-70\text{ }^{\circ}\text{C}$  and subsequent addition of Ph<sub>2</sub>PCl. After chromatographic purification 1 was obtained as a yellow solid with a yield of 41 %. The compound was characterized, and it agrees with the reported data [35]. The <sup>31</sup>P NMR spectrum, not described before, showed the expected singlet at  $-13.4\text{ ppm}$ .

The phosphane 1 is an air stable solid, but in aerated solution, is slowly converted to its oxide 2 upon daylight, while it is stable in the dark. A genuine sample of 2 was quantitatively prepared by intentional oxidation of 1 with H<sub>2</sub>O<sub>2</sub>. The phosphane sulfide 3 was obtained by treating 1 with sulfur in refluxing toluene. Both are yellow air stable solids and were readily characterized. The elemental analyses, yields, <sup>1</sup>H, and <sup>31</sup>P NMR spectroscopic data are collected in the Experimental Section. The <sup>31</sup>P NMR spectra showed a singlet low field shifted 46.2 or 55.6 ppm, respectively, compared to the phosphane. Compounds 1–3 are poorly soluble in organic solvents.

The gold(I) compounds [AuX(PPh<sub>2</sub>Per)] (X = Cl (4); X = C<sub>6</sub>F<sub>5</sub> (5)) and [AuX(SPPH<sub>2</sub>Per)] (6, 7) were easily prepared in good yield, as either orange (4–5) or yellow (6–7) solids, by 1:1 reaction in CH<sub>2</sub>Cl<sub>2</sub> of [AuX(tht)] (tht = tetrahydrothiophene) with the corresponding phosphane 2 or phosphane sulfide 3 (Scheme 1). The complexes were readily characterized by elemental analyses, yields, FTIR spectroscopy, <sup>1</sup>H, <sup>19</sup>F and <sup>31</sup>P NMR spectroscopic data, which are given in the Experimental

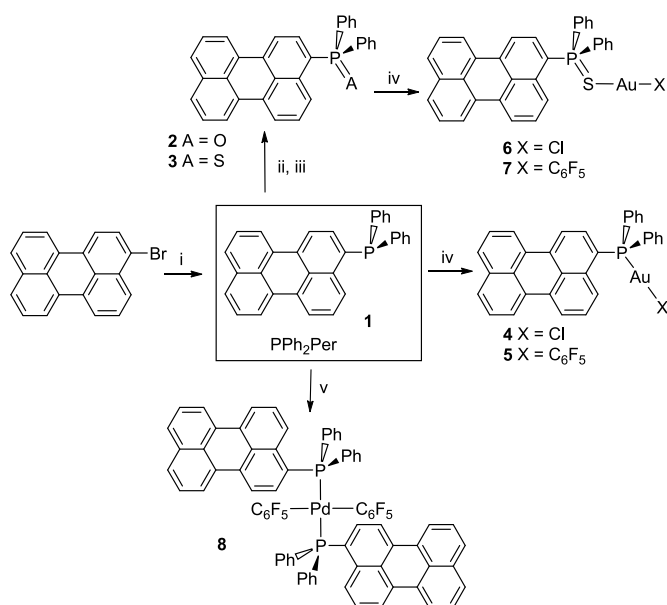
Section. The <sup>31</sup>P NMR spectra showed the expected singlet but low field shifted 39.9 (4) and 50.5 (5) ppm, or slightly shifted  $-0.4$  (6) and  $1.4$  (7) ppm, compared to the corresponding initial ligand. Therefore, they display singlets at 26.5 (4), 37.1 (5), 41.8 (6) and 43.6 (7) ppm. In the <sup>19</sup>F NMR spectra of compounds 5 and 7, the typical three resonances pattern (2F<sup>ortho</sup>: 1F<sup>para</sup>: 2F<sup>meta</sup>) for C<sub>6</sub>F<sub>5</sub> was observed. These gold complexes are moderately soluble in organic solvents commonly used, in any case more soluble than starting perylene ligands.

The reaction of PPh<sub>2</sub>Per with *trans*-[Pd(C<sub>6</sub>F<sub>5</sub>)<sub>2</sub>(SMe<sub>2</sub>)<sub>2</sub>] (molar ratio 2:1) in dichloromethane at room temperature afforded complex *trans*-[Pd(C<sub>6</sub>F<sub>5</sub>)<sub>2</sub>(PPh<sub>2</sub>Per)<sub>2</sub>] (8) as an orange solid. The <sup>31</sup>P (a singlet at 20.3 ppm) and <sup>19</sup>F NMR (F<sup>ortho</sup> at  $-111.9\text{ ppm}$ , F<sup>para</sup> at  $-162.0\text{ ppm}$  and F<sup>meta</sup> at  $-162.8\text{ ppm}$ ) spectra confirm the presence of only one isomer, and a *trans* arrangement of the two phosphanes is proposed to minimize the steric hindrance between the two bulky phosphane groups.

### 2.2. Crystal structures

X-ray quality crystals of gold complexes 5 and 7 allowed for the determination of their molecular structures by single-crystal X-ray diffraction methods. These are shown in Fig. 1 and Figs. S19–S20, and confirm the structures proposed in Scheme 1. Selected bond lengths and angles are given in Table 1, while the data collection and refinement parameters are detailed in the Supplementary Material.

The structures of 5 and 7 show the almost perfectly linear gold coordination with bond angle C–Au–P of 176.34(14)<sup>o</sup> for 5 and C–Au–S of 179.74(12)<sup>o</sup> for 7. The Au–S bond length in 7 (2.3036(15) Å) is longer than those found in [AuX(SPPH<sub>3</sub>)] (2.264 Å X = Cl, 2.286 Å X = Br), reflecting the high *trans*-influence of the pentafluorophenyl group [37]. The C–C–C angles at the ipso carbon of the C<sub>6</sub>F<sub>5</sub> group in both complexes are less than 120<sup>o</sup> (114.9(5) for 5 and 114.4(4)<sup>o</sup> for 7), a typical feature due to electronic effects of the electropositive metal and the electronegative fluorine substituents at the ortho positions [38]. In both complexes the perylene fragment is essentially planar and is almost perpendicular to the plane of C<sub>6</sub>F<sub>5</sub> moiety (96.26<sup>o</sup> for 5 and parallel for 7 (2.63<sup>o</sup>). The shortest Au...Au intermolecular distance between two metallic centers is 6.012 Å for 5 and 4.949 Å for 7, which clearly excludes any Au...Au interaction. However, there are significant  $\pi$ - $\pi$  interactions between the C<sub>6</sub>F<sub>5</sub> rings at a distance of 3.51 Å for 5 and 3.49 Å for 7 and between the perylene rings at 3.51 Å for 5 and 3.38 Å for 7 (Figs. S19–S20 in the Supplementary Material).



**Scheme 1.** Synthesis of PPh<sub>2</sub>Per derivatives: i) n-BuLi, THF ( $-70\text{ }^{\circ}\text{C}$ ); Ph<sub>2</sub>PPh; ii) H<sub>2</sub>O<sub>2</sub>; iii) S<sub>8</sub>; iv) [AuX(tht)]; v) *trans*-[Pd(C<sub>6</sub>F<sub>5</sub>)<sub>2</sub>(SMe<sub>2</sub>)<sub>2</sub>].

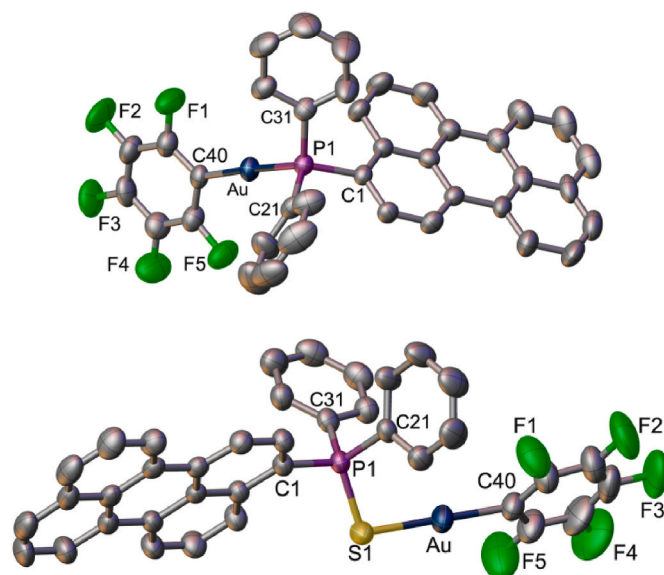


**Fig. 1.** Crystal structures of complexes 5 (CCDC2406214) and 7 (CCDC2406215) (H atoms are omitted for clarity).

**Table 1**  
Selected Interatomic Distances (Å) and Angles (°) for the complexes **5** and **7**.

	5	7
Au(1)–C(40)	2.058(5)	2.017(4)
Au(1)–P(1)	2.2835(17)	
Au(1)–S(1)		2.3036(15)
S(1)–P(1)		2.0183(15)
C(40)–Au(1)–P(1)	176.34(14)	
C(40)–Au(1)–S(1)		179.74(12)
C(31)–P(1)–C(21)	104.6(2)	105.76(15)
C(31)–P(1)–C(1)	105.9(2)	107.22(16)

## 2.3. Photophysical studies

### 2.3.1. UV–Vis absorption spectra

The UV–Vis absorption spectra of dilute solutions in chloroform ( $c \sim 10^{-5}$  M) of the precursors perylene, PPh<sub>2</sub>Per (**1**), OPPh<sub>2</sub>Per (**2**), SPPh<sub>2</sub>Per (**3**), and their complexes are shown in Fig. 2 (only one representative complex of each family is plotted to facilitate comparison; Figs. S22–S23 in the Supplementary Material show the spectra of all the compounds). Quantitative absorption data for all the compounds are summarized in Table 2.

All the spectra display two intense bands, a broad very intense one in the UV, at 240–315 nm (not shown in Fig. 2), and a second one, in the visible (350–500 nm), with a vibronic structure related to the  $\nu(\text{C}=\text{C})$  frequency of the perylene core and with increasing intensity of the vibronic bands for the higher  $\lambda$  value. The visible absorption of the perylene phosphane is a band ( $\lambda_{\text{max}}$  455 nm) covering the range 370–480 nm and red-shifted by about  $850 \text{ cm}^{-1}$  (17 nm) compared to perylene.

There is little change after oxidation or/and monodentate coordination of PPh<sub>2</sub>Per: the lower energy transition is slightly wider and has a shift maximum of  $286 \text{ cm}^{-1}$  (6 nm) without loss of the fine (vibronic) structure. This suggests that the electronic connection of the perylene and the metal fragments through the phosphane link is very weak (loss of the lone electron pair does not play a significant role in perturbing the perylenyl rings in the ligand). These bands show very little solvent dependence, less than  $240 \text{ cm}^{-1}$  (5 nm) for gold compound **4**, when the solvent changes from acetonitrile to toluene (see Fig. S21 in the Supplementary Material). Therefore, the band is tentatively assigned to a HOMO → LUMO transition centered in the perylene ligand. This will be discussed in more detail below, with the aid of DFT calculations.

Comparison of the UV–Vis absorption spectra of these perylene phosphane complexes with their pyrene analogues shows the effect of increased aromaticity of perylene: the absorption HOMO → LUMO of PPh<sub>2</sub>Per is less energetic ( $5800 \text{ cm}^{-1}$ ; 95 nm) [25]. The origin of these

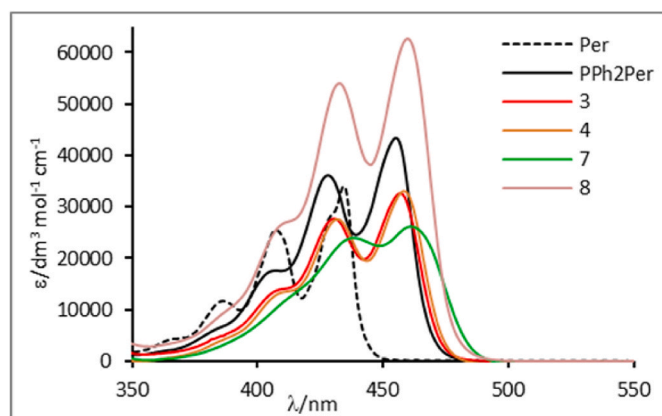


**Fig. 2.** Absorption spectra recorded in CHCl<sub>3</sub> solution ( $\sim 10^{-5}$  M) at room temperature: Perylene (Per), perylene phosphane (**1**), its sulfide (**3**) and selected Au<sup>I</sup> and Pd<sup>II</sup> complexes.

bands is discussed below, with the TD-DFT calculations. The UV–Vis spectra of phosphane ligand, their oxidized species and metallic complexes are studied in depth below, by DFT.

### 2.3.2. Molecular orbital calculations

A DFT study was performed to analyze and understand the absorption spectra of 3-perylenyldiphenylphosphane species. Computational details are given in the Experimental Section. The oxidized phosphanes P(V) are studied to understand the importance of donor atom bound to phosphorous, and followed to its coordination into gold complexes. Schematic representation of main expected transitions in the absorption spectra of **1–3** and chloro gold complexes **4** and **6** are shown in Fig. 3. Calculated absorption parameters, representation of molecular orbitals involved, main contributions for the transition and their coefficients are described in the Supplementary Material. Simulated UV–Vis spectra for these compounds are given in Table S3 in the Supplementary Material.

The absorption spectrum for the 3-perylenyldiphenylphosphane compound is dominated by two bands at 459 and 256 nm corresponding to perylene framework [39]. The first peak is assigned to HOMO → LUMO transition, and these two  $\pi$ -orbitals are basically centered in the perylene with a contribution of 94 and 98 %, respectively [40,41]. The second peak presents different single monoexcitations, in particular HOMO and higher empty orbital having 81 % of the perylene. The second band is less intense than the former, but it is enhanced by three extra bands at 259, 261 and 261 nm corresponding to diphenylphosphano fragment involving  $\pi$ -orbitals of the phenyl rings, resulting in two similar absorptions (simulated spectrum yields peaks at 459 and 260 nm). In the 3-perylenyldiphenylphosphane oxide, a blue-shift effect is observed for the two bands until 454 and 257 nm together an important decreasing of the absorbance, especially for the low wavelength peak. In opposition, they are redshifted for the 3-perylenyldiphenylphosphane sulfide to 459 and 258 nm, with a slight increasing of the absorbance than related phosphane oxide but not as high as those for the starting phosphane. We can notice that the second band is overlapping to a charge-transfer between sulfur lone pair to perylene  $\pi$ -system at 251 nm, and this can be related these changes with the electronegativities of oxygen and sulfur atoms bound to phosphorus.

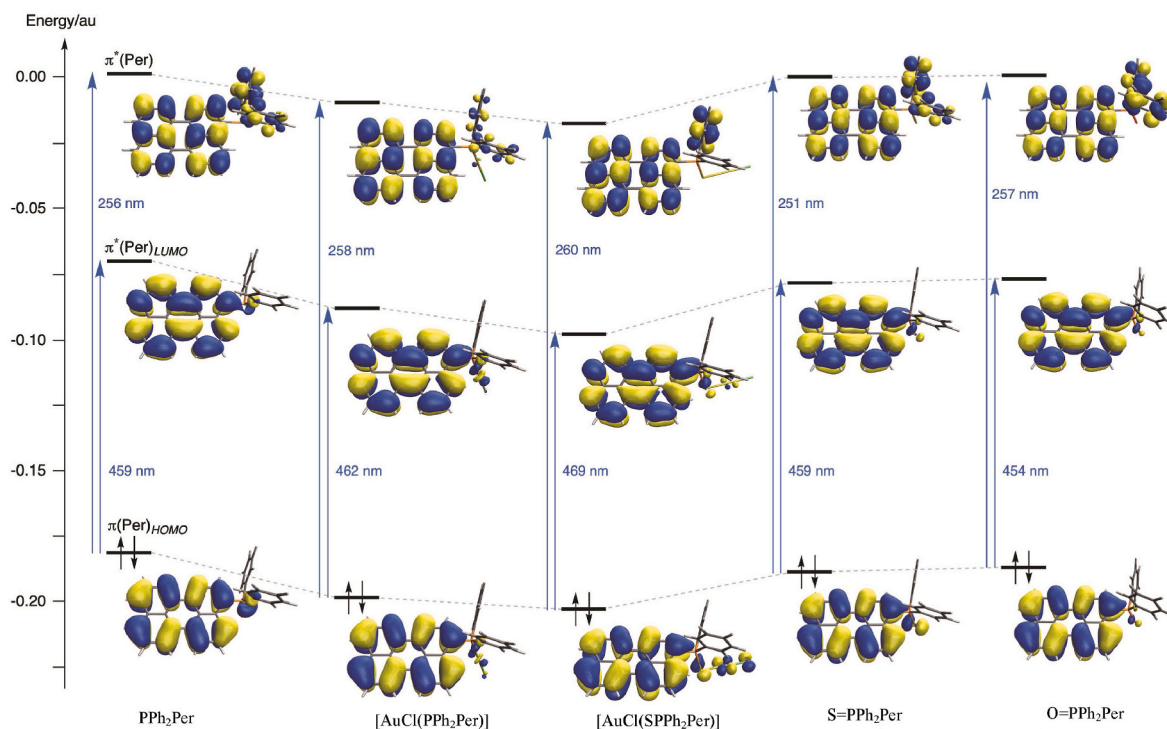
The coordination of both AuCl and Au(C<sub>6</sub>F<sub>5</sub>) fragments produces the same effect in related ligand, and consequently only the former is commented upon. The [AuCl(PPh<sub>2</sub>Per)] complex presents a small red-shift of HOMO → LUMO transition to 462 nm, while [AuCl(SPPh<sub>2</sub>Per)] one increases until 469 nm (taken the reference of both free ligands at 459 nm, respectively). In opposition, the coordination of gold fragments does not affect the second band, and it remains practically identical to uncoordinated species (258 and 260 nm, respectively). A detailed analysis of the molecular orbitals suggests small changes in their composition, although they are slightly stabilized by the coordination. However, it is important to point out a reduced participation of the  $\pi$ -system of the perylene into HOMO/LUMO is accompanied by an increase in the related wavelength. Moreover, it is remarkable a small band in the region between 290 and 310 nm for gold-sulfide derivatives that involve  $\pi$ -orbitals of the perylene as well as an ILCT from phosphano to perylene groups. Although this absorption is not well defined, a shoulder clearly appears in simulated spectrum due the coordination of the sulfur to the metal. Likewise, any monoexcitation involving perfluorophenyl is observed above 250 nm. The calculated values match reasonably with those found experimentally.

In summary, all these compounds display an intense low energy absorption band assigned to HOMO → LUMO transition, and both orbitals are dominated by perylene (90–96 %). In other studies some differences were observed, which could support the PET effect [39,42,43]. By carefully looking at the MOs involved in relevant electronic transitions in PPh<sub>2</sub>Per, the phosphano contributes mainly to several OM as HOMO-1 (43 % specifically from P atom) or LUMO+1, and this main contribution is lost for the rest of compounds (or moved to S or to C<sub>6</sub>F<sub>5</sub>).

Following the experimental work, we have studied complex [Pd

**Table 2**UV–Visible absorption and emission data for perylene phosphane (1), OPPh<sub>2</sub>Per (2), SPPPh<sub>2</sub>Per (3), and their complexes (4–8), in chloroform at 298 K.

Comp.	$\lambda$ (nm) ( $10^{-3} \epsilon$ )/ $\text{dm}^3 \text{mol}^{-1} \text{cm}^{-1}$	$\lambda_{\text{ex}}$ /nm	$\lambda_{\text{em}}^{\text{a}}$ /nm	Stokes shifts/ $\text{cm}^{-1}$	$\Phi_{\text{fl}}^{\text{b}}$ /%	$\tau^{\text{c}}$ /ns
PPh <sub>2</sub> Per	256 (46.4), 402 (16.5), 428 (36.1), 455 (43.3)	414, 440	468, 494	1359	13	4.49
2	259 (30.2), 403 (12.4), 428 (25.4), 454 (29.6)	433, 455	467, 488	565	83	4.89
3	259 (31.1), 406 (13.9), 430 (27.6), 457 (32.5)	433, 455	470, 500	701	71	4.37
4	270 (91.1), 407 (14.2), 431 (27.5), 457 (33.1)	433, 448	471, 497	1090	86	4.55
5	241 (36.3), 258 (28.9), 407 (14.2), 431 (29.4), 457 (35.3)	433, 453	470, 500	798	78	4.32
6	241 (22.1), 260 (26.3), 405 (10.3), 432 (21.1), 457 (24.3)	433, 453	471, 498	844	63	4.74
7	240 (28.5), 262 (45.2), 435 (23.9), 461 (26.1)	433, 454	471, 498	795	87	4.80
8	259 (77.4), 407 (25.2), 431 (53.9), 459 (62.6)	433, 453	472, 503	889	63	3.99

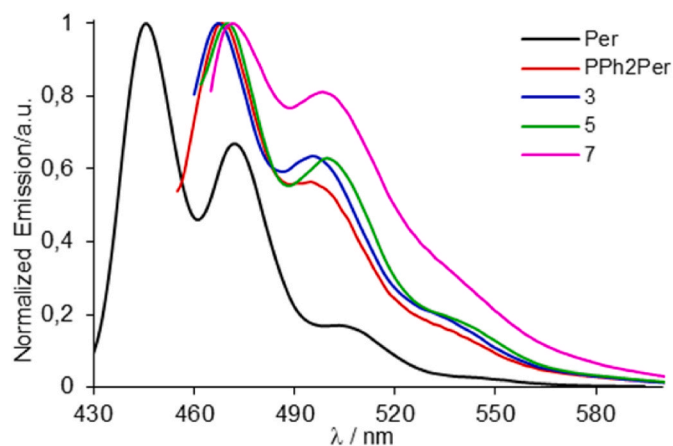
<sup>a</sup> Emission spectra collected by using  $\lambda_{\text{ex}}$  of 414 or 433 nm.<sup>b</sup> Quantum yield relative to perylene in ethanol ( $\Phi_{\text{fl}} = 92\%$ ).<sup>c</sup> Fluorescence lifetimes.**Fig. 3.** Schematic representation of main expected transitions in the absorption spectra of PPh<sub>2</sub>Per (1), [AuCl(PPh<sub>2</sub>Per)] (4), [AuCl(SPPPh<sub>2</sub>Per)] (6), SPPPh<sub>2</sub>Per (3), and OPPh<sub>2</sub>Per (2).

(C<sub>6</sub>F<sub>5</sub>)<sub>2</sub>(PPh<sub>2</sub>Per)<sub>2</sub>], which shows a large absorbance due that presence of two perylene groups, but their bands are split in two ranges, 487–450 and 262–260 nm, resulting maxima about 479 and 265 nm into simulated spectrum. A detailed analysis about two extra bands shows that these monoexcitations involve phenyl rings of the phosphano framework, being localized in this group (275 nm) or transference between perfluorophenyl to phosphano (293 nm).

### 2.3.3. Luminescence spectra

All the compounds are luminescent at room temperature in chloroform solution. The excitation and emission data are summarized in Table 2. The emission spectra of perylene, PPh<sub>2</sub>Per (1), OPPh<sub>2</sub>Per (2), SPPPh<sub>2</sub>Per (3), and their complexes are shown in Fig. 4 (only one representative complex of each family is plotted to facilitate comparison; Figs. S25–S26 in the Supplementary Material show the spectra of all the compounds).

The emission spectrum of PPh<sub>2</sub>Per shows one band in the range 450–550 nm and a red shift of 1360  $\text{cm}^{-1}$  (28 nm) compared to perylene. As observed in the absorption spectra, there is almost no change after oxidation or monodentate coordination of PPh<sub>2</sub>Per, and therefore

**Fig. 4.** Emission spectra recorded in CHCl<sub>3</sub> solution ( $10^{-5}$  M) at room temperature of: Perylene (Per), perylene phosphane (1), its sulfide (3) and selected Au<sup>I</sup> complexes.

compounds **2–8** exhibit only one band in the same range with only a maximum red shift up to  $182\text{ cm}^{-1}$  (4 nm). In summary, the emission maxima of perylene phosphane are slightly affected after oxidation, and coordination although the quantum yields are dramatically affected as we are going to explain below.

On the basis of the small Stokes shifts between absorption and emission and their emission lifetimes in the range 4.0–4.9 ns (Table 2), the luminescence observed can be assigned to  $\pi\text{--}\pi^*$  fluorescence. The emission properties remain unchanged in the presence of  $\text{O}_2$ , which is also consistent with this assignment. Most bands have a vibronic structure with a vibrational spacing of around  $1200\text{ cm}^{-1}$  related to the stretching C–C frequency of the perylene core, which suggests a perylene dominated emissive state that can be assigned as intraligand  $\pi\text{--}\pi^*$  disturbed by the  $\text{PPh}_2$  group. In addition, measurements for  $\text{PPh}_2\text{Per}$  **1** and gold complex **4** in several solvents with different polarity did not show change, which again suggests fluorescence due to the perylene moiety (See Fig. S24 in the Supplementary Data). Chloroform solutions are stable for weeks at room temperature and under natural light (except compound **1**, as explained above). In addition, these derivatives are soluble in dimethyl sulfoxide.

This emission behavior is similar to that found in phenanthrylphosphane cycloplatinated (II) and in group 11 compounds with 1,6-bis(diphenylphosphano)pyrene, which show only fluorescence [20, 27]. On the contrary, a related phenanthrylphosphane gold(I) complex exhibits blue-green room temperature phosphorescence ( $\Phi = 6\%$ ) [24], and in the same way pyrenylphosphane cycloplatinated (II) analogues display red phosphorescence (quantum yield up to 1.5 %) [25]. These works point out that phosphorescence in perylene systems is not an easy target due to the high and extensive  $\pi\text{--}\pi$  delocalization in perylene, which promotes frontier orbitals centered in the perylene moiety, and therefore fluorescence.

The emission quantum yields of  $\text{PPh}_2\text{Per}$  (**1**),  $\text{OPPh}_2\text{Per}$  (**2**),  $\text{SPPPh}_2\text{Per}$  (**3**), and their complexes were measured in chloroform at room temperature and the data are summarized in Table 2. The free ligand  $\text{PPh}_2\text{Per}$  (**1**) shows a quantum yield of 13 %, only a seventh that reported for perylene ( $\Phi_{\text{fl}} = 92\%$ ) [44]. However, after oxidation (**2–3**) or coordination to gold (**4–5**) or palladium (**8**) the quantum yield is recovered (63–86 %). Coordination of  $\text{SPPPh}_2\text{Per}$  (**3**) to gold (**6–7**) does not significantly affect the quantum yield. These facts can be related to a PET process: the lone electron pair in the phosphane interferes the perylene system and is therefore inhibited by oxidation or coordination to a metal fragment.

In summary, quantum yield exhibits a remarkable dependence on the phosphorus lone electron pair going from 13 % for the free phosphane to 63–87 % for oxidized forms or to 63–86 % for coordinated to gold or palladium.

### 3. Conclusions

We have prepared deep-colored phosphane perylene, its oxide and sulfide, as well as gold(I) and palladium(II) complexes. The electronic connection of the perylene and the phosphane substituents is very weak and therefore the absorption or emission maxima change slightly. However, the quantum yield is dramatically affected: the PET effect due to the lone electron pair of phosphane is inhibited by oxidation or coordination, going from 13 to 63–87 %, close to that found for unfunctionalized perylene (92 %). This approach can be applied not only in biosensing but also in chemosensing, expanding its potential for a wide range of applications in detecting biological and chemical targets.

## 4. Experimental Section

### 4.1. Materials and general methods

All reactions were carried out under dry nitrogen. The solvents were purified according to standard procedures. Literature methods were

used to prepare 3-bromoperylene [45],  $[\text{AuCl}(\text{tth})]$  [46],  $[\text{Au}(\text{C}_6\text{F}_5)(\text{tth})]$  [47],  $\text{trans-}[\text{Pd}(\text{C}_6\text{F}_5)_2(\text{SMe}_2)_2]$  [48]. C, H, N analyses were carried out on a PerkinElmer 2400 microanalyzer. Infrared spectra were measured on a PerkinElmer Frontier spectrometer coupled to a Pike GladiATR-210 accessory. Melting points were measured on a Gallenkamp apparatus and are uncorrected.  $^1\text{H}$  NMR,  $^{19}\text{F}$  NMR and  $^{31}\text{P}$  NMR spectra were recorded on a Varian 500 spectrophotometer in  $\text{CDCl}_3$ , with chemical shifts referred to TMS,  $\text{CFCl}_3$  and 85 %  $\text{H}_3\text{PO}_4$ , respectively. UV–Vis absorption spectra were obtained on a Shimadzu UV-1603 or UV-2550 spectrophotometer, in chloroform solution ( $1 \times 10^{-5}\text{ M}$ ). Luminescence data were recorded on a PerkinElmer LS-55 luminescence spectrometer, in  $\text{CHCl}_3$  ( $1 \times 10^{-5}\text{ M}$ ). Luminescence quantum yields were obtained at room temperature using the optically dilute method ( $A < 0.1$ ) in degassed chloroform (quantum yield standard was perylene in ethanol ( $\Phi_{\text{fl}} = 92\%$ ) [44]. The emission lifetime measurements were carried out with a Lifespec-red picosecond fluorescence lifetime spectrometer from Edinburgh Instruments. The technique used is “Time Correlated Single Photon Counting” (TCSPC).

### 4.2. Computational details

Unrestricted calculations were carried out using the Gaussian09 package [49]. The hybrid density function method known as B3LYP was applied [50]. Effective core potentials (ECP) were used to represent the innermost electrons of the transition atoms (Au and Pd) and the basis set of valence double- $\zeta$  quality for associated with the pseudopotentials known as LANL2DZ [51]. The basis set for the main group elements was 6-31G\* (C, N, O and H) [52,53]. Solvent effects of chloroform (or other solvents) were taken into account by PCM calculations [54], keeping the geometry optimized for gas phase (single-point calculations). Excited states and absorption spectra were obtained from the time-depending algorithm implemented in Gaussian09 [55].

### 4.3. Synthesis of $\text{PPh}_2\text{Per}$ (**1**)

To a solution of 3-bromoperylene (0.600 g, 1.81 mmol) in dry THF (60 mL) at  $-70\text{ }^\circ\text{C}$  was added dropwise a solution of 1.6 M  $n\text{BuLi}$  in hexane (1.35 mL, 2.17 mmol) and the resulting brown solution was stirred at  $-70\text{ }^\circ\text{C}$  (3 h), after which  $\text{P}(\text{C}_6\text{H}_5)_2\text{Cl}$  (0.33 mL, 1.81 mmol) was added, and the mixture was stirred for 3 h at  $-70\text{ }^\circ\text{C}$ . The solution was then allowed to warm up to room temperature and 0.5 mL of methanol was added. Then, the solvent was removed under vacuum and the residue was purified by column chromatography (silica gel, eluent  $\text{CH}_2\text{Cl}_2/\text{hexane}$  2:1) to give a yellow solid. Yield: 0.514 (65 %). Mp  $271\text{ }^\circ\text{C}$ . Found: C, 87.95; H, 4.75; molecular formula  $\text{C}_{32}\text{H}_{21}\text{P}$  requires C, 88.05; H, 4.85.  $^{31}\text{P}\{^1\text{H}\}$  NMR ( $\text{CDCl}_3$ ):  $\delta -13.4$  (s).

### 4.4. Synthesis of $\text{OPPh}_2\text{Per}$ (**2**)

To a solution of **1** (0.05 g, 0.11 mmol) in THF (10 mL) was added  $\text{H}_2\text{O}_2$  (0.1 mL, 30 %, 0.79 mmol) and the solution was stirred for 12 h at room temperature. The solvent was removed under vacuum and the residue was dissolved in dichloromethane (25 mL). The solution was dried ( $\text{MgSO}_4$ ), filtered, and the solvent removed under vacuum to give a yellow solid, which was washed with diethyl ether ( $2 \times 10\text{ mL}$ ). Yield: 0.034g (68 %). Mp  $343\text{ }^\circ\text{C}$  (decomp.). Found: C, 84.74; H, 4.65; molecular formula  $\text{C}_{32}\text{H}_{21}\text{OP}$  requires C, 84.94; H, 4.68.  $^1\text{H}$  NMR (500 MHz,  $\text{CDCl}_3$ ):  $\delta$  8.48 (d,  $J = 7.9\text{ Hz}$ , 1H), 8.27–8.20 (m, 3H), 8.08 (d,  $J = 7.9\text{ Hz}$ , 1H), 7.80–7.71 (m, 6H), 7.59 (t,  $J = 7.9\text{ Hz}$ , 2H), 7.56–7.44 (m, 8H).  $^{31}\text{P}\{^1\text{H}\}$  NMR ( $\text{CDCl}_3$ ):  $\delta$  32.8 (s).

### 4.5. Synthesis of $\text{SPPPh}_2\text{Per}$ (**3**)

Compound **1** (0.200 g, 0.45 mmol) and sulfur (0.015 g, 0.45 mmol) were refluxed in dry toluene (20 mL) for 5 h. The solvent was then evaporated under vacuum giving a yellow residue. This was purified by

column chromatography on silica gel using dichloromethane/hexane (2:1) as eluant. The second yellow band was collected, and the solvent evaporated under vacuum giving a yellow solid, which was washed with hexane ( $2 \times 3$  mL). Yield: 0.157 g (75 %). Mp 317 °C (decomp.). Rf ( $\text{CH}_2\text{Cl}_2$ /hexane (2:1), silica gel): 0.37. Found: C, 81.95; H, 4.45; molecular formula  $\text{C}_{32}\text{H}_{21}\text{PS}$  requires C, 82.03; H, 4.52.  $^1\text{H}$  NMR (500 MHz,  $\text{CDCl}_3$ ):  $\delta$  8.42 (d,  $J = 8.6$  Hz, 1H), 8.24–8.18 (m, 3H), 8.04 (dd,  $J = 8.0$ , 2.1 Hz, 1H), 7.94–7.86 (m, 4H), 7.78 (d,  $J = 8.0$  Hz, 1H), 7.74 (d,  $J = 8.0$  Hz, 2H), 7.59–7.48 (m, 8H), 7.41 (dd,  $J = 8.5$ , 7.6 Hz, 1H), 7.17 (dd,  $J = 16.1$ , 7.9 Hz, 1H).  $^{31}\text{P}\{^1\text{H}\}$  NMR ( $\text{CDCl}_3$ ):  $\delta$  42.2 (s).

#### 4.6. Synthesis of 4

This compound was obtained from the reaction of **1** (0.111 g, 0.25 mL) in dry  $\text{CH}_2\text{Cl}_2$  (25 mL) with  $[\text{AuCl}(\text{tht})]$  (0.081 g, 0.25 mmol). The reaction was stirred for 1 h at room temperature. The solvent was removed under reduced pressure, and the residual solid was purified by column chromatography on silica gel using dichloromethane as eluent. The solvent removed under vacuum to leave an orange solid which was washed with diethyl ether ( $2 \times 3$  mL). Yield 0.12 g (69 %). Mp 310 °C (decomp.). Rf ( $\text{CH}_2\text{Cl}_2$ /silica gel): 0.77. Found: C, 57.13; H, 2.99; molecular formula  $\text{C}_{32}\text{H}_{21}\text{AuP}$  requires C, 57.46; H, 3.16. FTIR: 330 ( $\text{Au}-\text{Cl}$ )  $\text{cm}^{-1}$ .  $^1\text{H}$  NMR (500 MHz,  $\text{CDCl}_3$ ):  $\delta$  8.30–8.21 (m, 3H), 8.18 (d,  $J = 7.5$  Hz, 1H), 8.04 (dd,  $J = 8.1$ , 1.7 Hz, 1H), 7.79 (d,  $J = 8.1$  Hz, 1H), 7.75 (d,  $J = 8.1$  Hz, 1H), 7.71–7.62 (m, 4H), 7.58 (dd,  $J = 7.5$ , 2.1 Hz, 2H), 7.56–7.42 (m, 7H), 6.97 (dd,  $J = 14.0$ , 7.9 Hz, 1H).  $^{31}\text{P}\{^1\text{H}\}$  NMR ( $\text{CDCl}_3$ ):  $\delta$  26.5 (s).

#### 4.7. Synthesis of 5

$[\text{Au}(\text{C}_6\text{F}_5)(\text{tht})]$  (0.049 g, 0.11 mmol) was reacted with **1** (0.050 g, 0.11 mmol) in dry  $\text{CH}_2\text{Cl}_2$  (10 mL) at room temperature for 1 h with stirring. The solvent was evaporated, and the residue was crystallized from dichloromethane/hexane to give an orange solid, which was washed with hexane ( $2 \times 5$  mL). Yield: 0.075 g (85 %). Mp 145 °C (decomp.). Found: C, 57.35; H, 3.15; molecular formula  $\text{C}_{38}\text{H}_{21}\text{AuF}_5\text{P}$  requires C, 57.02; H, 2.64. FTIR: 953, 808 ( $\text{C}_6\text{F}_5$ )  $\text{cm}^{-1}$ .  $^1\text{H}$  NMR (500 MHz,  $\text{CDCl}_3$ ):  $\delta$  8.53 (dd,  $J = 8.2$ , 1.6 Hz, 1H), 8.30 (d,  $J = 7.6$  Hz, 1H), 8.26 (d,  $J = 7.5$  Hz, 1H), 8.21 (d,  $J = 7.5$  Hz, 1H), 8.12 (dd,  $J = 7.9$ , 1.5 Hz, 1H), 7.82–7.65 (m, 6H), 7.61–7.49 (m, 9H), 7.04 (dd,  $J = 12.8$ , 7.9 Hz, 1H).  $^{31}\text{P}\{^1\text{H}\}$  NMR ( $\text{CDCl}_3$ ):  $\delta$  37.1 (s).  $^{19}\text{F}$  NMR ( $\text{CDCl}_3$ ):  $\delta$  -116.0 (m,  $2\text{F}^{\text{ortho}}$ ), -158.4 (t,  $J = 20.3$  Hz,  $1\text{F}^{\text{para}}$ ), -162.4 (m,  $2\text{F}^{\text{meta}}$ ).

#### 4.8. Synthesis of 6

To a solution of **3** (0.040 g, 0.085 mmol) in dry  $\text{CH}_2\text{Cl}_2$  (10 mL) was added  $[\text{AuCl}(\text{tht})]$  (0.027 g, 0.085 mmol). The workup was as **4** and a yellow solid was obtained. Yield: 0.051 g (86 %). Mp 193 °C (decomp.). Found: C, 54.39; H, 3.25; molecular formula  $\text{C}_{32}\text{H}_{21}\text{AuP}$  requires C, 54.83; H, 3.02. FTIR: 330 ( $\text{Au}-\text{Cl}$ )  $\text{cm}^{-1}$ .  $^1\text{H}$  NMR (500 MHz,  $\text{CDCl}_3$ ):  $\delta$  8.29–8.23 (m, 2H), 8.22 (d,  $J = 7.6$  Hz, 1H), 8.14–8.06 (m, 2H), 8.00–7.96 (m, 4H), 7.82 (d,  $J = 8.1$  Hz, 1H), 7.77 (d,  $J = 8.0$  Hz, 1H), 7.73–7.67 (m, 2H), 7.61–7.50 (m, 6H), 7.46 (t,  $J = 8.0$  Hz, 1H), 7.36 (dd,  $J = 17.1$ , 7.9 Hz, 1H).  $^{31}\text{P}\{^1\text{H}\}$  NMR ( $\text{CDCl}_3$ ):  $\delta$  41.8 (s).

#### 4.9. Synthesis of 7

To a solution of **3** (0.050 g, 0.108 mmol) in dry  $\text{CH}_2\text{Cl}_2$  (10 mL) was added  $[\text{Au}(\text{C}_6\text{F}_5)(\text{tht})]$  (0.027 g, 0.085 mmol). The workup was as **5** using dichloromethane/diethyl ether, and a yellow solid was obtained. Yield: 0.079 g (78 %). Mp 174 °C (decomp.). Found: C, 54.91; H, 2.50; molecular formula  $\text{C}_{38}\text{H}_{21}\text{AuF}_5\text{P}$  requires C, 54.82; H, 2.54. FTIR: 953, 808 ( $\text{C}_6\text{F}_5$ )  $\text{cm}^{-1}$ .  $^1\text{H}$  NMR (500 MHz,  $\text{CDCl}_3$ ):  $\delta$  8.28–8.24 (m, 3H), 8.16 (dd,  $J = 8.4$ , 0.9 Hz, 1H), 8.14–8.10 (m, 1H), 8.07–8.02 (m, 4H), 7.84 (d,  $J = 8.2$  Hz, 1H), 7.78 (d,  $J = 8.1$  Hz, 1H), 7.73–7.66 (m, 2H), 7.62–7.53 (m, 6H), 7.47 (dd,  $J = 8.5$ , 7.6 Hz, 1H), 7.40 (dd,  $J = 17.0$ , 8.0 Hz, 1H).

$^{31}\text{P}\{^1\text{H}\}$  NMR ( $\text{CDCl}_3$ ):  $\delta$  43.6 (s).  $^{19}\text{F}$  NMR ( $\text{CDCl}_3$ ):  $\delta$  -116.1 (m,  $2\text{F}^{\text{ortho}}$ ), -160.4 (t,  $J = 20.3$  Hz,  $1\text{F}^{\text{para}}$ ), -163.1 (m,  $2\text{F}^{\text{meta}}$ ).

#### 4.10. Synthesis of 8

*trans*- $[\text{Pd}(\text{C}_6\text{F}_5)_2(\text{SMe}_2)_2]$  (0.065 g, 0.11 mmol) was added to a solution of **1** (0.100 g, 0.23 mmol) in dry  $\text{CH}_2\text{Cl}_2$  (20 mL). The mixture was stirred at room temperature for 2 h. The workup was as for **4**, and an orange solid was obtained. Yield: 0.137 g (93 %). Mp 196 °C (decomp.). Found: C, 69.62; H, 3.27; molecular formula  $\text{C}_7\text{H}_4\text{F}_{10}\text{P}_2\text{Pd}$  requires C, 69.50; H, 3.22. FTIR: 953, 808 ( $\text{C}_6\text{F}_5$ )  $\text{cm}^{-1}$ .  $^1\text{H}$  NMR (500 MHz,  $\text{CDCl}_3$ ):  $\delta$  8.27 (d,  $J = 7.4$  Hz, 1H), 8.24–8.06 (m, 4H), 7.85 (d,  $J = 8.3$  Hz, 1H), 7.78 (d,  $J = 8.1$  Hz, 1H), 7.73 (d,  $J = 8.1$  Hz, 1H), 7.56–7.50 (m, 2H), 7.45–7.33 (m, 5H), 7.33–7.29 (m, 2H), 7.21–7.12 (m, 4H).  $^{31}\text{P}\{^1\text{H}\}$  NMR ( $\text{CDCl}_3$ ):  $\delta$  20.3 (s).  $^{19}\text{F}$  NMR ( $\text{CDCl}_3$ ):  $\delta$  -111.9 (m,  $4\text{F}^{\text{ortho}}$ ), -162.0 (t,  $J = 20.3$  Hz,  $2\text{F}^{\text{para}}$ ), -162.8 (m,  $4\text{F}^{\text{meta}}$ ).

#### 4.11. X-ray crystal structure analysis

Single crystals of **5** and **7** suitable for X-ray diffraction studies were obtained from slow diffusion of hexane into a chloroform solution for **5**, or diethyl ether into a dichloromethane solution for **7** of the products at -20 °C. Relevant crystallographic details are given in Table S1. Crystals were mounted in glass fibers, and diffraction measurements were made using a Bruker AXS SMART 1000 or a Varian Supernova area-detector diffractometer with  $\text{Mo-K}_\alpha$  radiation ( $\lambda = 0.71073$  Å). Intensities were integrated from several series of exposures, each exposure covering  $0.3^\circ$  in  $\omega$ , the total data set being a hemisphere. Absorption corrections were applied, based on multiple and symmetry-equivalent measurements. The structures were solved and refined by least squares on weighted  $F^2$  values for all reflections (see Table S1) by using the Olex2 software including the Shelx software [56,57]. The non-hydrogen atoms were refined anisotropically and hydrogen atoms were placed at idealized positions and refined using the riding model. A solvent mask was calculated to substitute half disordered  $\text{CHCl}_3$  molecule in compound **5**. Crystallographic data (excluding structure factors) for the structures reported in this paper have been deposited with the Cambridge Crystallographic Data Centre as Supplementary publications with deposition numbers CCDC2406214 for **5**, and CCDC2406215 for **7**.

#### CRedit authorship contribution statement

**J. Emilio Expósito**: Investigation. **Sergio Lentijo**: Investigation, Formal analysis. **Gabriel Aullón**: Writing – original draft, Investigation, Funding acquisition, Formal analysis. **Manuel Bardají**: Writing – review & editing, Writing – original draft, Visualization, Formal analysis. **Jesús A. Miguel**: Writing – review & editing, Writing – original draft, Supervision, Funding acquisition, Conceptualization.

#### Data availability

The research data are included as supplementary material.

#### Declaration of competing interest

The authors declare that they have no known competing financial interests or personal relationships that could have appeared to influence the work reported in this paper.

#### Acknowledgements

Financial support for this work was provided by grant PID2023-148145OA-I00 funded by MICIU/AEI/10.13039/501100011033 and by “ERDF/EU”; by the Spanish Structures of Excellence María de Maeztu program (CEX2021-001202-M) and by the *Generalitat de Catalunya* through grant 2021SGR 286. The measurements were carried out in part

in the Laboratory of Instrumental Techniques (LTI) Research Facilities, Universidad de Valladolid.

## Appendix A. Supplementary data

Supplementary data to this article can be found online at <https://doi.org/10.1016/j.dyepig.2025.112690>.

## Data availability

No data was used for the research described in the article.

## References

- Zollinger H. *Color chemistry*. third ed. Weinheim: Wiley-VCH; 2003.
- Würthner F., Thalacker C., Diele S., Tschierske C. Fluorescent J-type aggregates and thermotropic columnar mesophases of perylene bisimide dyes. *Chem Eur J* 2001;7:2245–2253. doi: [https://chemistry-europe.onlinelibrary.wiley.com/doi/10.1002/1521-3765\(20010518\)7:10%3C2245::AID-CHEM2245%3E3.0.CO;2-W](https://chemistry-europe.onlinelibrary.wiley.com/doi/10.1002/1521-3765(20010518)7:10%3C2245::AID-CHEM2245%3E3.0.CO;2-W).
- Chen Z, Baumeister U, Tschierske C, Würthner F. Effect of core twisting on self-assembly and optical properties of perylene bisimide dyes in solution and columnar liquid crystalline phases. *Chem Eur J* 2007;13:450–65. <https://doi.org/10.1002/chem.200600891>.
- Schmidt-Mende L, Fechtenkötter A, Müllen K, Moons E, Friend R, MacKenzie JD. Self-organized discotic liquid crystals for high-efficiency organic photovoltaics. *Science* 2001;293:1119–22. <https://www.science.org/doi/10.1126/science.293.5532.1119>.
- Chen S, Slattum P, Wang C, Zang L. Self-assembly of perylene imide molecules into 1D nanostructures: methods, morphologies, and applications. *Chem Rev* 2015;115:11967–98. <https://doi.org/10.1021/acs.chemrev.5b00312>.
- Gsänger M, Bialas D, Huang L, Stolte M, Würthner F. Organic semiconductors based on dyes and color pigments. *Adv Mater* 2016;28:3615–45. <https://doi.org/10.1002/adma.201505440>.
- Harris DH, Brixi S, Gelfand BS, Lessard BH, Welch GC. A N–H functionalized perylene diimide with strong red–light absorption for green solvent processed organic electronics. *J Mater Chem C* 2020;8:9811–5. <https://doi.org/10.1039/D0TC02284E>.
- Padghan SD, Chung MC, Zhang QS, Lin WC, Chen KY. 1,6,7–Trisubstituted perylene bisimides with tunable optical properties for colorimetric and “turn-on” fluorescence detection of HCl. *Dyes Pigments* 2022;202:110303. <https://doi.org/10.1016/j.dyepig.2022.110303>.
- Erkan A, Volkan B, Canan V. Tuning the colour of solution processed perylene tetraester based OLEDs from yellowish–green to greenish–white: a molecular engineering approach. *Dyes Pigments* 2023;211:111050. <https://doi.org/10.1016/j.dyepig.2022.111050>.
- Würthner F, Kaiser TE, Saha–Möller CR. J–Aggregates: from serendipitous discovery to supramolecular engineering of functional dye materials. *Angew Chem Int Ed Engl* 2011;50:3376–410. <https://doi.org/10.1002/anie.201002307>.
- Herbst S, Soberats B, Leowanawat P, Lehmann M, Würthner F. A columnar liquid–crystal phase formed by hydrogen–bonded perylene bisimide J–aggregates. *Angew Chem Int Ed Engl* 2017;56:2162–5. <https://doi.org/10.1002/anie.201612047>.
- Domínguez C, Baena MJ, Coco S, Espinet P. Perylenecarboxydiimide–gold(I) organometallic dyes. Optical properties and Langmuir films. *Dyes Pigments* 2017; 140:375–83. <https://doi.org/10.1016/j.dyepig.2017.01.057>.
- Imwiset KJ, Ogawa M. Highly luminescent inorganic–organic hybrids with molecularly dispersed perylene. *Inorg Chem* 2021;60:9563–70. <https://doi.org/10.1021/acs.inorgchem.1c00701>.
- Valente G, Esteve–Rochina M, Alves SPC, Martinho JMG, Ortí E, Calbo J, et al. Perylene–based coordination polymers: synthesis, fluorescent J–aggregates, and electrochemical properties. *Inorg Chem* 2023;62:7834–42. <https://doi.org/10.1021/acs.inorgchem.3c00540>.
- Sharma P, Venugopal A, Martínez Verdi C, Serra Roger M, Calò A, Kumar M. Heparin binding induced supramolecular chirality into the self-assembly of perylenediimide bolaamphiphile. *J Mater Chem B* 2024;12:7292–7. <https://doi.org/10.1039/D4TB00862F>.
- Baumgartner T, Réau R. Organophosphorus  $\pi$ -conjugated materials. *Chem Rev* 2006;106:4681–727. <https://doi.org/10.1021/cr040179m>.
- Fey N, Orpen AG, Harvey JN. Building ligand knowledge bases for organometallic chemistry: computational description of phosphorus(III)–donor ligands and the metal–phosphorus bond. *Coord Chem Rev* 2009;253:704–22. <https://doi.org/10.1016/j.ccr.2008.04.017>.
- Burt J, Levason W, Reid G. Coordination chemistry of the main group elements with phosphine, arsine and stibine ligands. *Coord Chem Rev* 2014;260:65–115. <https://doi.org/10.1016/j.ccr.2013.09.020>.
- Han C, Xie G, Xu H, Zhang Z, Yan P, Zhao Y, et al. Xanthene–based phosphine oxide host with the planar multi–insulating structure for efficient electrophosphorescence. *Dyes Pigments* 2012;94:561–9. <https://doi.org/10.1016/j.dyepig.2012.03.013>.
- Hu J, Lin R, Yip JHK, Wong KY, Ma DL, Vittal JJ. Synthesis and electronic spectroscopy of luminescent cyclometalated Platinum–Anthracenyl complexes. *Organometallics* 2007;26:6533–43. <https://doi.org/10.1021/om700706r>.
- Schillmöller T, Ruth PN, Herbst–Irmer R, Stalke D. Three colour solid–state luminescence from positional isomers of facily modified thiophosphoranyl anthracenes. *Chem Commun* 2020;56:7479–82. <https://doi.org/10.1039/D0CC02585B>.
- Benítez M, Buil ML, Esteruelas MA, López AM, Martín–Escura C, Oñate E. C–H, N–H, and O–H bond activations to prepare phosphorescent hydride–iridium(III)–Phosphine emitters with photocatalytic achievement in C–C coupling reactions. *Inorg Chem* 2024;63:6346–61. <https://doi.org/10.1021/acs.inorgchem.4c00115>.
- Rawe BW, Brown CM, MacKinnon MR, Patrick BO, Bodwell GJ, Gates DP. A C–pyrenyl poly(methylenephosphine): oxidation “turns on” blue photoluminescence in solution and the solid state. *Organometallics* 2017;36: 2520–6. <https://doi.org/10.1021/acs.organomet.6b00880>.
- Osawa M, Hoshino M, Akita M, Wada T. Synthesis and characterization of phenanthrylphosphine gold complex: observation of Au–induced blue–green phosphorescence at room temperature. *Inorg Chem* 2005;44:1157–9. <https://doi.org/10.1021/ic048538j>.
- Hu J, Yip JHK, Ma DL, Wong KY, Chung WH. Switching on the phosphorescence of pyrene by cycloplatination. *Organometallics* 2009;28:51–9. <https://doi.org/10.1021/om800410m>.
- Heng WY, Hu J, Yip JHK. Attaching gold and platinum to the rim of pyrene: a synthetic and spectroscopic study. *Organometallics* 2007;26:6760–8. <https://doi.org/10.1021/om700716p>.
- Hu J, Nguyen MH, Yip JHK. Metallocyclophanes of 1,6–Bis(diphenylphosphino) pyrene: excimeric emission and effect of oxygen on stability of the rings. *Inorg Chem* 2011;50:7429–39. <https://doi.org/10.1021/ic102441b>.
- Monot J, Marelli E, Martin–Vaca B, Bourissou D. (P,C)–cyclometalated complexes derived from naphthyl phosphines: versatile and powerful tools in organometallic chemistry. *Chem Soc Rev* 2023;52:3543–66. <https://doi.org/10.1039/D2CS00564>.
- Pandey R, Kumar A, Xu Q, Pandey DS. Zinc(ii), copper(ii) and cadmium(ii) complexes as fluorescent chemosensors for cations. *Dalton Trans* 2020;49:542–68. <https://doi.org/10.1039/C9DT03017D>.
- Liu X, Qi Y, Pu S, Wang Y, Gao Z. Sensing mechanism of a new fluorescent probe for hydrogen sulfide: photoinduced electron transfer and invalidity of excited–state intramolecular proton transfer. *RSC Adv* 2021;11:22214–20. <https://doi.org/10.1039/D1RA02511B>.
- Xu W, Wu P, Li X, Liu S, Feng L, Xiong H. Two birds with one stone: a highly sensitive near–infrared BODIPY–based fluorescent probe for the simultaneous detection of Fe<sup>2+</sup> and H<sup>+</sup> in vivo. *Talanta* 2021;233:122601. <https://doi.org/10.1016/j.talanta.2021.122601>.
- Dong Y, Fan R, Chen W, Wang P, Yang Y. A simple quinolone Schiff–base containing CHEF based fluorescence “turn-on” chemosensor for distinguishing Zn<sup>2+</sup> and Hg<sup>2+</sup> with high sensitivity, selectivity and reversibility. *Dalton Trans* 2017; 46:6769–75. <https://doi.org/10.1039/C7DT00956A>.
- Tian X, Murfin LC, Wu L, Lewis SE, James TD. Fluorescent small organic probes for biosensing. *Chem Sci* 2021;12:3406–26. <https://doi.org/10.1039/D0SC06928K>.
- Wu ZH, Zhu X, Yang Q, Zagranyarski Y, Mishra K, Strickfaden H, et al. Near–Infrared perylenecarboximide fluorophores for live–cell super–resolution imaging. *J Am Chem Soc* 2024;146:7135–9. <https://doi.org/10.1021/jacs.3c13368>.
- Chotimarkorn C, Nagasaka R, Ushio H, Ohshima T, Matsunaga S. Development of novel fluorescent probe 3–perylene diphenylphosphine for determination of lipid hydroperoxide with fluorescent image analysis. *Biochem Biophys Res Commun* 2005;338:1222–8. <https://doi.org/10.1016/j.bbrc.2005.10.060>.
- Chotimarkorn C, Ohshima T, Ushio H. Fluorescent image analysis of lipid hydroperoxides in fish muscle with 3–perylene diphenylphosphine. *Lipids* 2006;41: 295–300. <https://doi.org/10.1007/s11745-006-5100-z>.
- Hussain MS, Isab AA, Saded A, Al–Arfaj AR. Crystal structure of bromotri(phenyl) phosphinesulphide–gold(I), (C<sub>6</sub>H<sub>5</sub>)<sub>3</sub>PSAuBr. *Z Kristallogr - New Cryst Struct* 2001; 216:629–30. <https://doi.org/10.1524/nocrs.2001.216.14.663>.
- Jones PG. The distortion of pentafluorophenyl groups in metal complexes: limitations of rigid–body refinement. *J Organomet Chem* 1988;345:405–11. [https://doi.org/10.1016/0022-328X\(88\)80103-7](https://doi.org/10.1016/0022-328X(88)80103-7).
- Expósito JE, Aullón G, Bardají M, Miguel JA, Espinet P. Fluorescent perylenylpyridine complexes: an experimental and theoretical study. *Dalton Trans* 2020;49:13326–38. <https://doi.org/10.1039/D0DT02494E>.
- Expósito JE, Aullón G, Alvarez–Paíno M, Miguel JA, Espinet P. Higher fluorescence in platinum(IV) orthometalated complexes of perylene imine compared with their platinum(II) or palladium(II) analogues. *Dalton Trans* 2015;44:16164–76. <https://doi.org/10.1039/C5DT02572A>.
- Lentijo S, Expósito JE, Aullón G, Miguel JA, Espinet P. Highly fluorescent complexes with 3–isocyanoperylene and N–(2,5–di–tert–butylphenyl)–9–isocyanoperylene–3,4–dicarboximide. *Dalton Trans* 2014;43:10885–97. <https://doi.org/10.1039/C4DT01016G>.
- Song FQ, Cheng H, Zhao NN, Song XQ. Construction of enhanced fluorescence sensors in aqueous media by cation regulation and hybridization. *J Lumin* 2021; 239:118338. <https://doi.org/10.1016/j.jlumin.2021.118338>.
- Kajjam AB, Singh K, Tej RVV, Vaidyanathan S. Carbazole–acenaphthene (donor–acceptor)–based luminophores for picric acid detection: a combined experimental and theoretical study. *Mater Adv* 2021;2:5236–47. <https://doi.org/10.1039/D1MA000445J>.
- Montalti M, Credi A, Prodi L, Gandolfini MT. *Handbook of photochemistry*. third ed. Boca Raton, FL: CRC Pres LLC; 2005. <https://doi.org/10.1201/9781420015195>.

- [45] Mitchell RH, Lai YH, Williams RV. N-Bromosuccinimide–dimethylformamide: a mild, selective nuclear monobromination reagent for reactive aromatic compounds. *J Org Chem* 1979;44:4733–5. <https://doi.org/10.1021/jo00393a066>.
- [46] Usón R, Laguna A, Laguna M. (Tetrahydrothiophene)Gold(I) or gold(III) complexes. *Inorg Synth* 1989;26:85–91. <https://doi.org/10.1002/9780470132579.ch17>.
- [47] Usón R, Laguna A, Vicente J. Preparation and properties of stable salts containing mono- or bis-(pentafluorophenyl)aurate(I) and mono-, tris-, or tetrakis-(pentafluorophenyl)aurate(III) ions. *J Chem Soc Chem Commun* 1976:353–4. <https://doi.org/10.1039/C39760000353>.
- [48] Espinet P, Martínez-Illarduya JM, Pérez-Briso C, Casado AL, Alonso MA. 3,5-dichlorotrifluorophenyl complexes, aryl derivatives with simple <sup>19</sup>F NMR structural probes. The synthesis of general precursors for Pd- and Pt complexes. *J Organomet Chem* 1998;551:9–20. [https://doi.org/10.1016/S0022-328X\(97\)00424-5](https://doi.org/10.1016/S0022-328X(97)00424-5).
- [49] Frisch MJ, Trucks GW, Schlegel HB, Scuseria GE, Robb MA, Cheeseman JR, et al. *Gaussian 09 (revision B.1)*. Wallingford CT: Gaussian Inc.; 2010.
- [50] Becke AD. Density-functional thermochemistry. III. The role of exact exchange. *J Chem Phys* 1993;98:5648–52. <https://doi.org/10.1063/1.464913>.
- [51] Hay PJ, Wadt WR. Ab initio effective core potentials for molecular calculations. Potentials for K to Au including the outermost core orbitals. *J Chem Phys* 1985;82:299–310. <https://doi.org/10.1063/1.448975>.
- [52] Hariharan PC, Pople JA. The influence of polarization functions on molecular orbital hydrogenation energies. *Theoret Chim Acta* 1973;28:213–22. <https://doi.org/10.1007/BF00533485>.
- [53] Francl MM, Pietro WJ, Hehre WJ, Binkley JS, Gordon MS, DeFrees DJ, Pople JA. Self-consistent molecular orbital methods. XXIII. A polarization-type basis set for second-row elements. *J Chem Phys* 1982;77:3654–65. <https://doi.org/10.1063/1.444267>.
- [54] Amovilla C, Barone V, Cammi R, Cancès E, Cossi M, Mennucci B, et al. Recent advances in the description of solvent effects with the polarizable continuum model. *Adv Quant Chem* 1998;32:227–61. [https://doi.org/10.1016/S0065-3276\(08\)60416-5](https://doi.org/10.1016/S0065-3276(08)60416-5).
- [55] Casida ME, Jamorski C, Casida KC, Salahub DR. Molecular excitation energies to high-lying bound states from time-dependent density-functional response theory: characterization and correction of the time-dependent local density approximation ionization threshold. *J Chem Phys* 1998;108:4439–49. <https://doi.org/10.1063/1.475855>.
- [56] Dolomanov OV, Bourhis JL, Gildea RJ, Howard JAK, Puschmann H. OLEX2: a complete structure solution, refinement and analysis program. *J Appl Cryst* 2009;42:339–41. <https://doi.org/10.1107/S0021889808042726>.
- [57] Sheldrick GM. Shelxt - integrated space-group and crystal-structure determination. *Acta Cryst A* 2015;C71:3–8. <https://doi.org/10.1107/s2053273314026370>.